Journal of Power Sources 202 (2012) 225–229

Contents lists available at SciVerse ScienceDirect

Journal of Power Sources

journal homepage: www.elsevier.com/locate/jpowsour

Short communication

Performance of Ni–Fe/gadolinium-doped CeO_2 anode supported tubular solid oxide fuel cells using steam reforming of methane

Bo Liang[a,*], Toshio Suzuki[a], Koichi Hamamoto[a], Toshiaki Yamaguchi[a], Hirofumi Sumi[a], Yoshinobu Fujishiro[a], Brian J. Ingram[b], John David Carter[b]

[a] National Institute of Advanced Industrial Science and Technology, Nagoya, Japan
[b] Argonne National Laboratory, Argonne, IL, USA

ARTICLE INFO

Article history:
Received 1 November 2011
Received in revised form
24 November 2011
Accepted 24 November 2011
Available online 2 December 2011

Keywords:
SOFC
Methane
Carbon fiber
Micro tube

ABSTRACT

Iron nanoparticles (Fe_2O_3) were added to NiO/gadolinium-doped CeO_2 (GDC) anode supported solid oxide fuel cell (SOFC) for the direct methane–water fuel operation. The cell was co-sintered at 1400 °C, and the anode porosity is 31.8%. The main size corresponding to peak volume is around 1.5 μm. When steam and methane directly fed to the cell, the power density is about 0.57 W cm^{-2} at 650 °C. It is the familiar performance for H_2 operation (4 times of flow rate) with same fuel utilization. Compare with the testing temperature of 600 and 650 °C, there is almost no carbon fiber deposition at 700 °C with steam/methane (S/C) of 5. At the same time, fuel operation of high value of S/C (=3.3) resulted in fiber-like deposition and degradation of power performance based on loading test results.

© 2011 Elsevier B.V. All rights reserved.

1. Introduction

Solid oxide fuel cells (SOFCs) convert the chemical energy of fuel directly into electricity and heat [1]. The working temperature expands from 600 °C to 1000 °C depending on electrodes, electrolyte as well as the microstructure [2–8]. Most fuel cells often use hydrogen as the fuel, but more applications need to use the easily available fuels, such as methane. Present demonstration of fuel-cell therefore included a reformer which converts hydrocarbon fuel into hydrogen. However, high operating temperature makes SOFCs as power source without a reformer. They can use methane fuel directly to generate energy.

On the other hand, high operating temperatures limit the types of materials that can be used in the cell and decrease the mechanical strength due to discrepant expansion [9]. So, an intermediate temperature range is more desired in SOFC using hydrocarbon as fuel. At intermediate operating temperatures, ceria-based materials showed significantly higher ionic conductivity than yttrium-stabilized zirconia (YSZ). Furthermore, it enhanced direct oxidation of hydrocarbons due to rapid lattice oxygen mobility [10,11]. Also, pure-ceria (CeO_2) was used as functional layer to direct reformation of hydrocarbon fuel [12].

Comparison of the electrochemical activities of Mn, Fe, Co, Ni, Ru, and Pt showed that Ni has the highest activity for hydrogen oxidation at intermediate temperature [13]. However, carbon deposition happened severely on the nickel surface, which is caused by pyrolysis reaction or the Boudouard reaction [14,15]. To avoid this problem, other metals such as copper were added in Ni-cermet anode [16]. However, copper is not stable above 1100 °C (m.p. = 1083 °C), while high sintering temperatures are required to fabricate a high quality SOFC. Furthermore, it is famous that the addition of ruthenium (Ru) to Ni–GDC is also effective for methane oxidation while inhibiting carbon deposition [17]. However, a part of the added Ru was lost from the anode surface due to its vaporization at elevated temperatures. Due to high melting point, Ni–Fe bimetal has been investigated as an electron conductor [18–20]. At the same time, in our previous work the microstructure will be optimized by adding some amount of Fe to a standard Ni/GDC cell [21]. The porosity was high, and the pores in anode were three-dimensionally connected.

In this study, Ni–Fe/GDC tubular cells were investigated using steam/methane as fuel. The cells were tested at various operating temperatures, and for different steam/methane. The microstructure and surface morphology of the cells were shown using field emission scanning electron microscopy (FE-SEM). The cell performance was discussed with the impedance results, anode porosity, together with microstructure of anode.

* Corresponding author. Tel.: +81 527367581; fax: +81 527367405.
E-mail address: basafan@gmail.com (B. Liang).

0378-7753/$ – see front matter © 2011 Elsevier B.V. All rights reserved.
doi:10.1016/j.jpowsour.2011.11.070

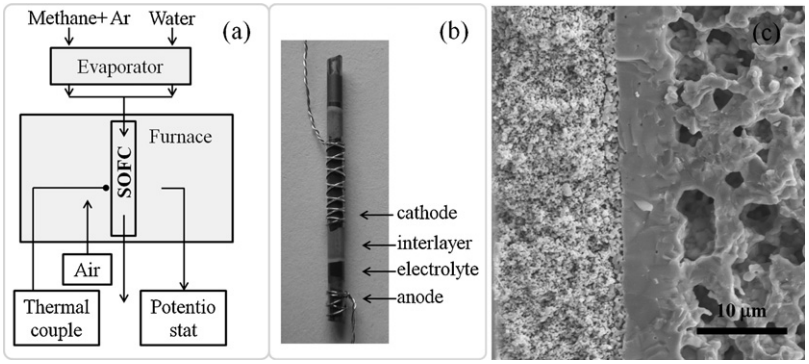

Fig. 1. (a) Experimental apparatus for testing single tubular cell. (b) Real image of a SOFC using Fe_2O_3–NiO/GDC anode supported. (c) Cross-sectional fracture SEM image of the microtubular cell.

2. Experimental

2.1. Fabrication of microtubular solid oxide fuel cell

NiO–Fe_2O_3/GDC anode tube was made by mixing of NiO and Fe_2O_3 powder (Ni:Fe is 9:1 by mol), GDC powder, poly methyl methacrylate beads (PMMA), and binder. These powders were mixed for 1 h by a mixer, 5DMV-r, and after adding proper amount of water; it was stirred for 30 min in a vacuum chamber. The mixture (clay) was aged for 15 h. Then, anode tubes were extruded from a metal mold by using a piston cylinder type extruder (Ishikawa-Toki Tekko-sho Co., Ltd.). Using co-sintering process, a very thin ScSZ electrolyte around 5 μm was securely fabricated on the anode tubes. In detail, the electrolyte layer was dip-coated on the anode tube using ScSZ (Daiichiki-genso Co., Ltd.) slurry. The slurry consisted of ScSZ powder, binder as well as organic ingredients (toluene and ethanol), and the weight ratio is 10:1:15. The coated film on anode tube was dried, then, the anode–electrolyte were co-sintered 1400 °C for 1 h in the air. They were again dip-coated using GDC slurry and sintered at 1200 °C. The GDC slurry consisted of GDC powder, binder and organic ingredients with weight ratio of 10:1:14. Next, the anode tubes with electrolyte (ScSZ) and interlayer (GDC) were dip-coated in cathode slurry. This cathode slurry consisted of $La_{0.6}Sr_{0.4}Co_{0.2}Fe_{0.8}O_{3-y}$ (LSCF), GDC powders (weight ratio to LSCF is 3:1) as well as organic ingredients. Organic ingredients were similar with those of the electrolyte slurry. After dip-coating the cathode slurry, the tubes were dried and sintered at 1050 °C for 1 h in the air to complete a cell.

2.2. Characterization

The performance of the cell was investigated using an experimental apparatus which is shown in Fig. 1(a). The Fe_2O_3-containing anode is shown in Fig. 1(b) and (c). They respectively give the real image of a cell and the cross-sectional view of the specific part from anode to cathode. The cell was co-sintered at 1400 °C. In our previous work [22], 1400 °C prefers to co-sinter a high quality cell with dense electrolyte, although the porosity of anode is slightly lower than 1300 and 1350 °C. The tubular cell was sealed at an alumina tube using a ceramic sealing paste. Ag wires were used for collecting current of the anode and cathode sides, which were both fixed by painting a colloidal silver paste. Diluted methane (10% CH_4 in Ar) mixed with steam was flowed inside of the tubular cell. Cathode side was open to the air. The size of the cell was about 1.85 mm in diameter, 30 mm in tube length. The active cathode area is 0.5–0.6 cm^2. The pores volume of anode sintering at 1400 °C was obtained by mercury porosimeter. Open circuit voltage, *I–V* plots, and EIS plots were collected using a multichannel potentiostat (Solartron 1260 frequency response analyzer with a 1296 Interface) based on two chamber configuration. The tubular cells were tested at the temperature of 600, 650 and 700 °C, which were tested by a thermocouple placed closed to the cell.

Table 1
The particle size used in anode–electrolyte. *D*50 is particle diameter value in case cumulative distribution percentage reaches 50%.

	ScSZ	GDC	Fe_2O_3	NiO	PMMA
*D*50 (μm)	0.62	0.63	0.05	0.1	5

3. Results and discussion

Table 1 provides the size of particles (GDC, NiO, Fe_2O_3, PMMA bead, ScSZ) used in the anode support and electrolyte. It is because that the co-sintering behavior partly depends on the particle size of them.

Fig. 2 shows the microstructure and porous properties of anode before reducing. As can be seen, the accumulated volume consists of the pores with size of 0.1–1.5 μm which be considered the pores between grains. The NiO–Fe_2O_3/GDC anode tube has pores volume of 0.073 cc g^{-1}, and its porosity is 31.8%. The pore size corresponding to the peak of volume fraction is around 1.5 μm. More important, these pores are three-dimensionally connected, which will prefer the fast gas diffusion.

Fig. 3(a) shows the performance of the micro tubular cells operating at various temperatures: 500, 550, 600, 650 and 700 °C. The fuel gas flow rate is 22.5 mL min^{-1} (10% CH_4 + 90% Ar) which mixed with 11.2 mL min^{-1} steam. As can be seen, the maximum power density of the cells is respectively 0.04, 0.13, 0.36, 0.56, and 0.75 W cm^{-2}. Furthermore, as shown in Fig. 3(b), the maximum power density using methane almost equals hydrogen at the

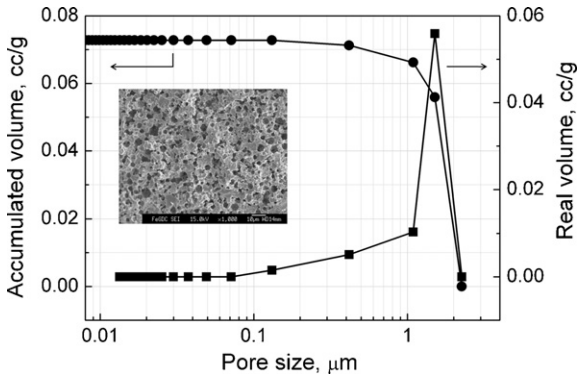

Fig. 2. The cumulative volume and pore size distribution of the anode support before the test. The inset shows the microstructure of anode support.

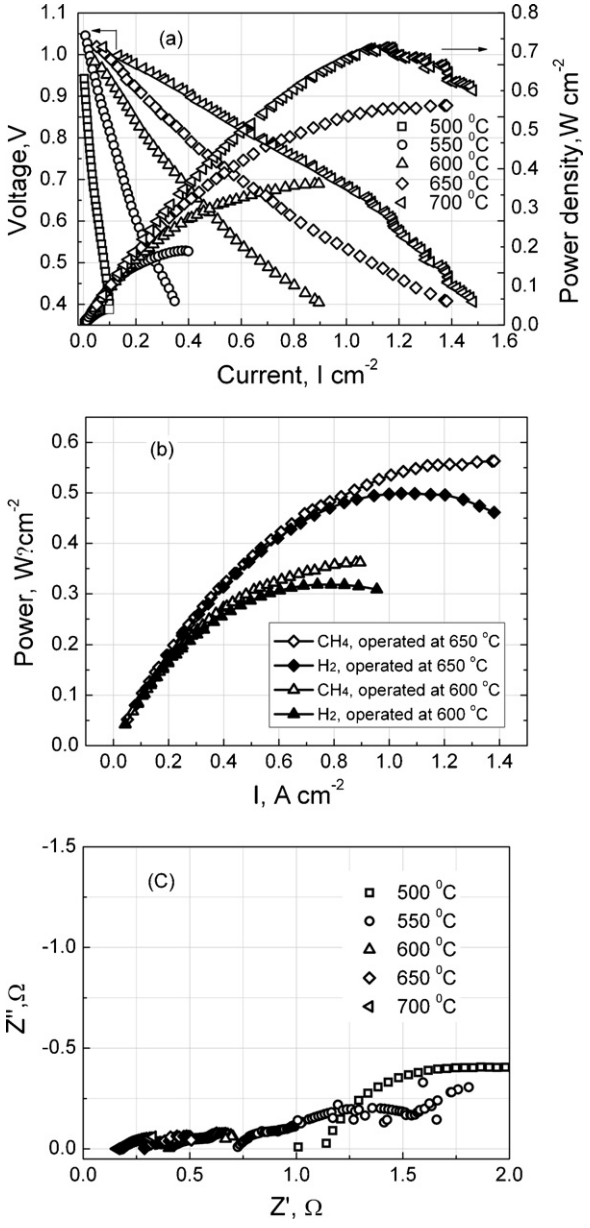

Fig. 3. (a) Results of voltage and power density versus current density at various temperatures, performed on the tubular cell using methane. (b) Cell performance obtained at different temperatures using H_2/Ar and steam/methane (S/C = 5). (c) Impedance spectra of the cell corresponding to the conditions of (a), which were recorded in the frequency range from 1 Hz to 1 MHz.

temperatures of 600 °C and 650 °C. The corresponding fuel flow rates are 2.25 mL min^{-1} for pure CH_4 and 9.5 mL min^{-1} for pure H_2. So, from the point of fuel utilization of view, methane reacts efficiently with oxygen ions in a porous Ni–Fe cermet anode even without a gas reforming system. The performance of the cell showed almost no difference for methane fuel and 4 times of H_2 fuel. Fig. 3(c) shows impedance spectra of the cells which corresponded to Fig. 3(a). The impedance was recorded near the open circuit voltage. As clearly be seen, the low frequency semi-circles decreased as operating temperature increasing. So, the cell with 31.8% anode porosity is good for fuel diffusing.

Fig. 4 shows the FE-SEM images of anode tube (inner surface) after 4 h testing. The cells were operated at various temperatures: 600 °C, 650 °C and 700 °C. With a loading current density of 0.4 A cm^{-2}, all the operations were done using steam/methane without a reformer. Running the cell with S/C = 5 (steam at flow rate of 11.2 cc min^{-1}) shows little deposition at 600 and 650 °C. They are fiber-like structure. However, the deposition almost disappeared at 700 °C. Keeping the same steam flow rate, the cells were tested at 650 °C with S/C = 3.3 to investigate the effect of fuel concentration. Fig. 5 shows the morphology of the cell (inner surface of anode tube) operated for different S/C (3.3 and 5). The loading current density is same, and it is 0.4 A cm^{-2}. As can be seen, when S/C increased from 5 to 3.3, more deposition was observed on the inner surface of anode tube. Surface morphology indicated that fiber-like structures densely deposited on the surface of metal particles (Ni and Fe). No deposition was founded on GDC grains where looks relatively smooth.

Fig. 6 shows the FE-SEM images of anode tubes (fuel outlet) and its corresponding EDS results. The cell was operated at 650 °C for 4 h. From the EDS results in Fig. 6(b), it was known the deposition consisted of carbon. Also, we analyzed element composition of two fibers across the red lines. (For interpretation of the references to color in the text, the reader is referred to the web version of the article.) As can be seen, two carbon signal peaks appeared at the positions which corresponded to the two crossings between red line and fibers. When the red line went up, both the two crossings and the two signal peaks became closed to each other. Finally, two signal peaks merge as one when the two carbon fibers crossed at the top. So, carbon fibers were deposited on Ni–Fe bimetal anode tube for some operations such as low testing temperature and low S/C (=3.3).

In order to investigate how the S/C and carbon deposition affected the cell performance, loading tests were carried out. Fig. 7 just shows the results of 5200 s, because the difference can be clearly seen. The cell was tested at 650 °C and the loading current density is 0.4 A cm^{-2}. As can be seen, there was clear difference of voltages changing. With the same output current, the voltages of the cell is almost table (0.79 V) for the operation of S/C = 5, while there was about 0.03 V decreasing (from 0.85 V to 0.82 V) for the operation of S/C = 3.3. It is possibly because of the carbon fiber deposition. At the temperature around 650 °C, carbon deposition

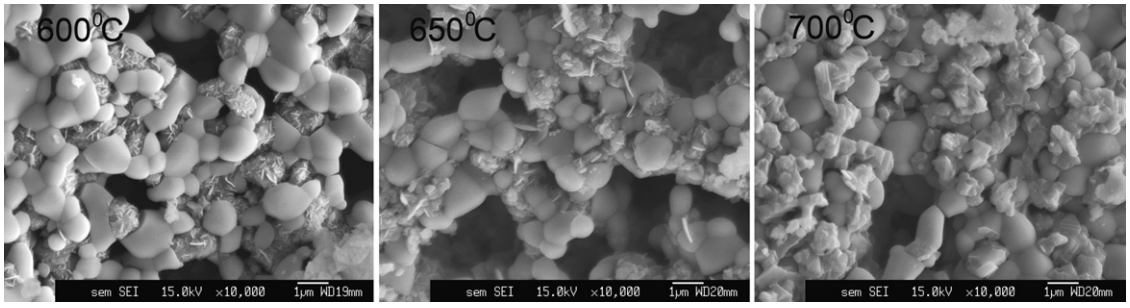

Fig. 4. FE-SEM images for Ni–Fe/GDC anodes after power generation (4 h). The cell was tested at various temperatures, and steam/methane is 5.

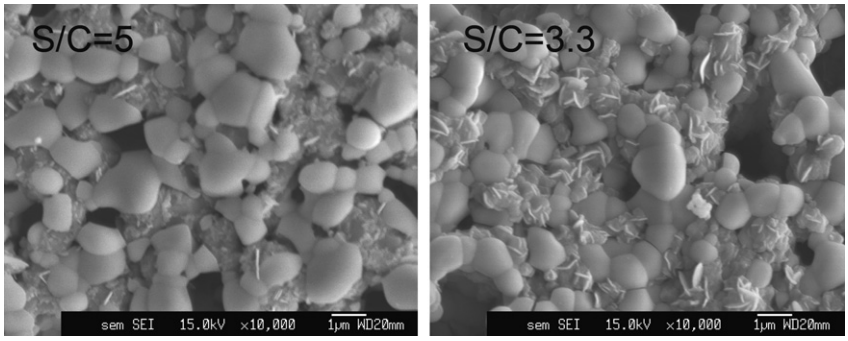

Fig. 5. FE-SEM images for Ni–Fe/GDC anodes after power generation at 650 °C (4 h). The cell operated for different S/C.

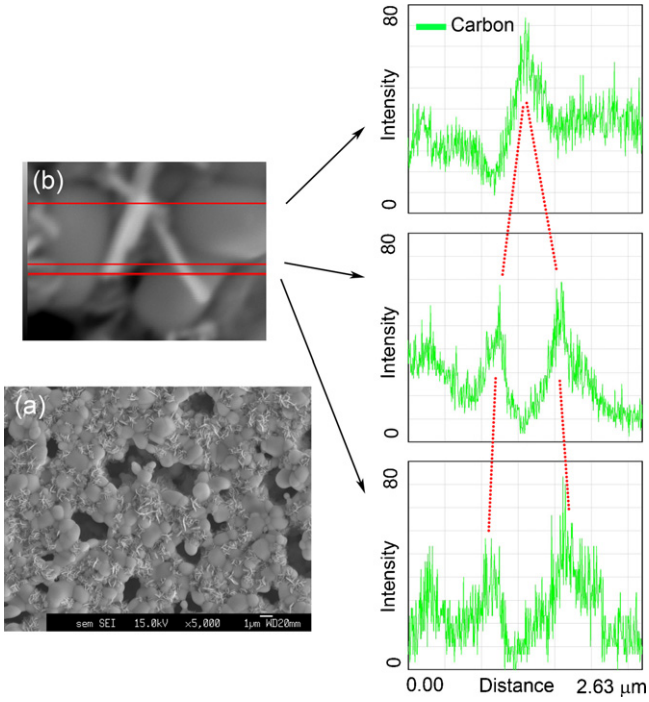

Fig. 6. (a) Morphology of the inner surface of anode tube after measurement at 650 °C. The fuel is steam/methane with S/C = 3.3. (b) Backscattered electron images of selective spot in (a) and the corresponding linear EDS spectrum for carbon fiber at different place.

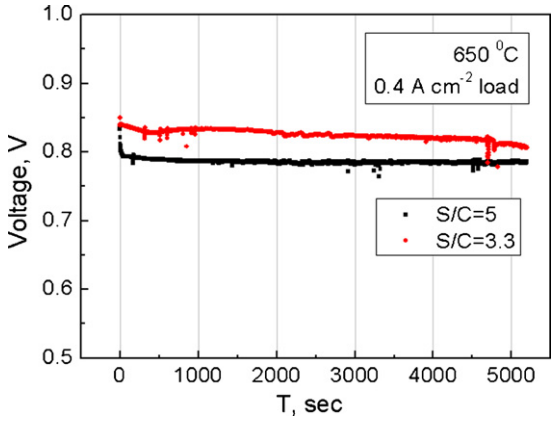

Fig. 7. The results of loading test at first stage, 0.4 A cm^{-2}, at 650 °C for different S/C.

is mainly formed via the pyrolysis reaction [10]. But the reaction rate is very slow without catalysts such as Ni. In this study, 30% weight of anode tube is from Ni and Fe. The surface-seated nickel and iron particles are also believed to be a good catalyst for carbon nanowalls deposition [23]. The deposited carbon fibers weaken the anode catalytic ability and clogged the pores of the anode. Furthermore, compare with low S/C (=3), S/C (=5) produces high H_2 concentration and low hydrocarbon concentration [24]. Therefore, at the operation of low S/C, more carbon deposition existed and the performance of the cell degraded. In short, operating a cell (tubular structure) for high value of S/C (5) can decrease the carbon deposition (as shown in Fig. 4), and achieve stable power performance.

4. Conclusion

In the study, Ni–Fe/GDC tubular SOFCs were investigated at different values of S/C and temperatures. Adding some amount of Fe (Fe:Ni is 1:9 by mol) to standard Ni/GDC anode tube will affect the co-sintering process of anode–electrolyte. The cell showed similar performance with H_2 fuel (4 times flow rate to methane) when methane/H_2O was directly fed to the cell. At the operating temperature of 700 °C (for S/C = 5), there was almost no carbon fibers deposition on anode and the maximum power density was about 0.75 W cm^{-2}. At the same time, fuel operation of high value of S/C (=3.3) resulted in more fiber-like deposition than that of high S/C (=5). Loading test results showed high value of S/C (=5) is suggested to be used for the system utilizing hydrocarbon/steam as fuel.

Acknowledgment

This work is supported by Japan-US Clean Energy Technologies Development.

References

[1] A.B. Stambouli, E. Traversa, Renew. Sust. Energy Rev. 6 (2002) 433–455.
[2] S. Pinol, M. Morales, F. Espiell, J. Power Sources 169 (2007) 2–8.
[3] C. Kleinlogel, L.J. Gauckler, Solid State Ionics 135 (2000) 567–573.
[4] R.O. Fuentes, R.T. Baker, Int. J. Hydrogen Energy 33 (2008) 3480–3484.
[5] S.R. Wang, H. Inaba, H. Tagawa, T. Hashimoto, J. Electrochem. Soc. 144 (1997) 4076–4080.
[6] T. Hibino, A. Hashinoto, T. Inoue, J.I. Tokuno, S.I. Yoshida, J. Electrochem. Soc. 147 (2000) 2888–2892.
[7] S.W. Zha, W. Rauch, M.L. Liu, Solid State Ionics 166 (2004) 241–250.
[8] T. Suzuki, Z. Hasan, Y. Funahashi, T. Yamaguchi, Y. Fujishiro, M. Awano, Science 325 (2009) 852–855.
[9] T. Hibino, A. Hashimoto, K. Asano, M. Yano, M. Suzuki, M. Sano, Electrochem. Solid-State Lett. 5 (2002) A242–A244.
[10] W. Zhu, C.R. Xia, J. Fan, R.R. Peng, G.Y. Meng, J. Power Sources 160 (2006) 897–902.
[11] S.W. Jung, C. Lu, H.P. He, K.Y. Ahn, R.J. Gorte, J.M. Vohs, J. Power Sources 154 (2006) 42–50.
[12] T. Suzuki, T. Yamaguchi, K. Hamamoto, Y. Fujishiro, M. Awano, N. Sammes, Energy Environ. Sci. 4 (2011) 940–943.

[13] T. Setoguchi, K. Okamoto, K. Eguchi, H. Arai, J. Electrochem. Soc. 139 (1992) 2875–2880.
[14] E. Perry Murray, T. Tsai, S.A. Barnett, Nature 400 (1999) 649–651.
[15] J.B. Wang, H.C. Jang, T.J. Huang, J. Power Sources 122 (2003) 122–131.
[16] S. Park, J.M. Vohs, R.J. Gorte, Nature 404 (2000) 265–267.
[17] T. Hibino, A. Hashimoto, M. Yano, M. Suzuki, M. Sano, Electrochim. Acta 48 (2003) 2531–2537.
[18] Y.W. Ju, S. Ida, T. Inagaki, T. Ishihara, J. Power Sources 196 (2011) 6062–6069.
[19] R.d.P. Fiuza, M.A.d. Silva, J.S. Boaventura, Int. J. Hydrogen Energy 35 (2010) 11216–11228.
[20] H. Kan, H.J. Lee, Catal. Commun. 12 (2010) 36–39.
[21] B. Liang, T. Suzuki, K. Hamamoto, T. Yamaguchi, Y. Fujishiro, M. Awano, B.J. Ingram, J.D. Cater, Int. J. Hydrogen Energy 36 (2011) 10975–10980.
[22] B. Liang, T. Suzuki, K. Hamamoto, T. Yamaguchi, Y. Fujishiro, M. Awano, B.J. Ingram, J.D. Cater, J. Power Sources 196 (2011) 9124–9129.
[23] Y. Wu, P. Qiao, T. Chong, Z. Shen, Adv. Mater. 14 (2002) 64–67.
[24] T. Suzuki, T. Yamaguchi, Y. Fujishiro, M. Awano, T. Kikuchi, A. Fujii, Y. Funahashi, J. Fuel Cell Sci. Technol. 8 (2011) 011008–11014.